The Astrophysical Journal, 710:1271–1285, 2010 February 20 doi:10.1088/0004-637X/710/2/1271

SPECTRAL PROPERTIES OF BRIGHT *FERMI*-DETECTED BLAZARS IN THE GAMMA-RAY BAND

A. A. Abdo[1,2], M. Ackermann[3], M. Ajello[3], W. B. Atwood[4], M. Axelsson[5,6], L. Baldini[7], J. Ballet[8], G. Barbiellini[9,10], D. Bastieri[11,12], K. Bechtol[3], R. Bellazzini[7], B. Berenji[3], R. D. Blandford[3], E. D. Bloom[3], E. Bonamente[13,14], A. W. Borgland[3], A. Bouvier[3], J. Bregeon[7], A. Brez[7], M. Brigida[15,16], P. Bruel[17], T. H. Burnett[18], S. Buson[11], G. A. Caliandro[19], R. A. Cameron[3], P. A. Caraveo[20], S. Carrigan[12], J. M. Casandjian[8], E. Cavazzuti[21], C. Cecchi[13,14], Ö. Çelik[22,23,24], E. Charles[3], A. Chekhtman[1,25], C. C. Cheung[1,2], J. Chiang[3], S. Ciprini[14], R. Claus[3], J. Cohen-Tanugi[26], J. Conrad[6,27,56], S. Cutini[21], C. D. Dermer[1], A. de Angelis[28], F. de Palma[15,16], S. W. Digel[3], E. do Couto e Silva[3], P. S. Drell[3], R. Dubois[3], D. Dumora[29,30], C. Farnier[26], C. Favuzzi[15,16], S. J. Fegan[17], W. B. Focke[3], P. Fortin[17], M. Frailis[28,31], Y. Fukazawa[32], S. Funk[3], P. Fusco[15,16], F. Gargano[16], D. Gasparrini[21], N. Gehrels[22,33,34], S. Germani[13,14], B. Giebels[17], N. Giglietto[15,16], P. Giommi[21], F. Giordano[15,16], T. Glanzman[3], G. Godfrey[3], I. A. Grenier[8], M.-H. Grondin[29,30], J. E. Grove[1], L. Guillemot[29,30,35], S. Guiriec[36], A. K. Harding[22], R. C. Hartman[22], M. Hayashida[3], E. Hays[22], S. E. Healey[3], D. Horan[17], R. E. Hughes[37], M. S. Jackson[6,38], G. Jóhannesson[3], A. S. Johnson[3], W. N. Johnson[1], T. Kamae[3], H. Katagiri[32], J. Kataoka[39], N. Kawai[40,41], M. Kerr[18], J. Knödlseder[42], M. Kuss[7], J. Lande[3], L. Latronico[7], M. Lemoine-Goumard[29,30], F. Longo[9,10], F. Loparco[15,16], B. Lott[29,30,57], M. N. Lovellette[1], P. Lubrano[13,14], G. M. Madejski[3], A. Makeev[1,25], M. N. Mazziotta[16], W. McConville[22,34], J. E. McEnery[22,34], C. Meurer[6,27], P. F. Michelson[3], W. Mitthumsiri[3], T. Mizuno[32], A. A. Moiseev[23,34], C. Monte[15,16], M. E. Monzani[3], A. Morselli[43], I. V. Moskalenko[3], S. Murgia[3], P. L. Nolan[3], J. P. Norris[44], E. Nuss[26], T. Ohsugi[32], N. Omodei[7], E. Orlando[45], J. F. Ormes[44], D. Paneque[3], J. H. Panetta[3], D. Parent[1,25,29,30], V. Pelassa[26], M. Pepe[13,14], M. Persic[9,31], M. Pesce-Rollins[7], F. Piron[26], T. A. Porter[4], S. Rainò[15,16], R. Rando[11,12], M. Razzano[7], A. Reimer[3,46], O. Reimer[3,46], T. Reposeur[29,30], S. Ritz[4,4], L. S. Rochester[3], A. Y. Rodriguez[19], R. W. Romani[3], M. Roth[18], F. Ryde[6,38], H. F.-W. Sadrozinski[4], D. Sanchez[17], A. Sander[37], P. M. Saz Parkinson[4], J. D. Scargle[47], C. Sgrò[7], E. J. Siskind[48], D. A. Smith[29,30], P. D. Smith[37], G. Spandre[7], P. Spinelli[15,16], M. S. Strickman[1], D. J. Suson[49], H. Tajima[3], H. Takahashi[32], T. Takahashi[50], T. Tanaka[3], J. B. Thayer[3], J. G. Thayer[3], D. J. Thompson[22], L. Tibaldo[8,11,12,58], D. F. Torres[19,51], G. Tosti[13,14], A. Tramacere[3,52], Y. Uchiyama[3], T. L. Usher[3], V. Vasileiou[23,24], N. Vilchez[42], M. Villata[53], V. Vitale[43,54], A. P. Waite[3], P. Wang[3], B. L. Winer[37], K. S. Wood[1], T. Ylinen[6,38,55], and M. Ziegler[4]

[1] Space Science Division, Naval Research Laboratory, Washington, DC 20375, USA
[2] National Research Council Research Associate, National Academy of Sciences, Washington, DC 20001, USA
[3] W. W. Hansen Experimental Physics Laboratory, Kavli Institute for Particle Astrophysics and Cosmology, Department of Physics and SLAC National Accelerator Laboratory, Stanford University, Stanford, CA 94305, USA
[4] Santa Cruz Institute for Particle Physics, Department of Physics and Department of Astronomy and Astrophysics, University of California at Santa Cruz, Santa Cruz, CA 95064, USA
[5] Department of Astronomy, Stockholm University, SE-106 91 Stockholm, Sweden
[6] The Oskar Klein Centre for Cosmoparticle Physics, AlbaNova, SE-106 91 Stockholm, Sweden
[7] Istituto Nazionale di Fisica Nucleare, Sezione di Pisa, I-56127 Pisa, Italy
[8] Laboratoire AIM, CEA-IRFU/CNRS/Université Paris Diderot, Service d'Astrophysique, CEA Saclay, 91191 Gif sur Yvette, France
[9] Istituto Nazionale di Fisica Nucleare, Sezione di Trieste, I-34127 Trieste, Italy
[10] Dipartimento di Fisica, Università di Trieste, I-34127 Trieste, Italy
[11] Istituto Nazionale di Fisica Nucleare, Sezione di Padova, I-35131 Padova, Italy
[12] Dipartimento di Fisica "G. Galilei," Università di Padova, I-35131 Padova, Italy
[13] Istituto Nazionale di Fisica Nucleare, Sezione di Perugia, I-06123 Perugia, Italy
[14] Dipartimento di Fisica, Università degli Studi di Perugia, I-06123 Perugia, Italy
[15] Dipartimento di Fisica "M. Merlin" dell'Università e del Politecnico di Bari, I-70126 Bari, Italy
[16] Istituto Nazionale di Fisica Nucleare, Sezione di Bari, 70126 Bari, Italy
[17] Laboratoire Leprince-Ringuet, École polytechnique, CNRS/IN2P3, Palaiseau, France
[18] Department of Physics, University of Washington, Seattle, WA 98195-1560, USA
[19] Institut de Ciencies de l'Espai (IEEC-CSIC), Campus UAB, 08193 Barcelona, Spain
[20] INAF-Istituto di Astrofisica Spaziale e Fisica Cosmica, I-20133 Milano, Italy
[21] Agenzia Spaziale Italiana (ASI) Science Data Center, I-00044 Frascati (Roma), Italy
[22] NASA Goddard Space Flight Center, Greenbelt, MD 20771, USA
[23] Center for Research and Exploration in Space Science and Technology (CRESST) and NASA Goddard Space Flight Center, Greenbelt, MD 20771, USA
[24] Department of Physics and Center for Space Sciences and Technology, University of Maryland Baltimore County, Baltimore, MD 21250, USA
[25] George Mason University, Fairfax, VA 22030, USA
[26] Laboratoire de Physique Théorique et Astroparticules, Université Montpellier 2, CNRS/IN2P3, Montpellier, France
[27] Department of Physics, Stockholm University, AlbaNova, SE-106 91 Stockholm, Sweden
[28] Dipartimento di Fisica, Università di Udine and Istituto Nazionale di Fisica Nucleare, Sezione di Trieste, Gruppo Collegato di Udine, I-33100 Udine, Italy
[29] CNRS/IN2P3, Centre d'Études Nucléaires Bordeaux Gradignan, UMR 5797, Gradignan, 33175, France
[30] Université de Bordeaux, Centre d'Études Nucléaires Bordeaux Gradignan, UMR 5797, Gradignan, 33175, France
[31] Osservatorio Astronomico di Trieste, Istituto Nazionale di Astrofisica, I-34143 Trieste, Italy
[32] Department of Physical Sciences, Hiroshima University, Higashi-Hiroshima, Hiroshima 739-8526, Japan
[33] Department of Astronomy and Astrophysics, Pennsylvania State University, University Park, PA 16802, USA
[34] Department of Physics and Department of Astronomy, University of Maryland, College Park, MD 20742, USA
[35] Max-Planck-Institut für Radioastronomie, Auf dem Hügel 69, 53121 Bonn, Germany
[36] Center for Space Plasma and Aeronomic Research (CSPAR), University of Alabama in Huntsville, Huntsville, AL 35899, USA
[37] Department of Physics, Center for Cosmology and Astro-Particle Physics, The Ohio State University, Columbus, OH 43210, USA
[38] Department of Physics, Royal Institute of Technology (KTH), AlbaNova, SE-106 91 Stockholm, Sweden

[39] Research Institute for Science and Engineering, Waseda University, 3-4-1, Okubo, Shinjuku, Tokyo 169-8555, Japan
[40] Department of Physics, Tokyo Institute of Technology, Meguro City, Tokyo 152-8551, Japan
[41] Cosmic Radiation Laboratory, Institute of Physical and Chemical Research (RIKEN), Wako, Saitama 351-0198, Japan
[42] Centre d'Étude Spatiale des Rayonnements, CNRS/UPS, BP 44346, F-30128 Toulouse Cedex 4, France
[43] Istituto Nazionale di Fisica Nucleare, Sezione di Roma "Tor Vergata," I-00133 Roma, Italy
[44] Department of Physics and Astronomy, University of Denver, Denver, CO 80208, USA
[45] Max-Planck Institut für extraterrestrische Physik, 85748 Garching, Germany
[46] Institut für Astro- und Teilchenphysik and Institut für Theoretische Physik, Leopold-Franzens-Universität Innsbruck, A-6020 Innsbruck, Austria
[47] Space Sciences Division, NASA Ames Research Center, Moffett Field, CA 94035-1000, USA
[48] NYCB Real-Time Computing Inc., Lattingtown, NY 11560-1025, USA
[49] Department of Chemistry and Physics, Purdue University Calumet, Hammond, IN 46323-2094, USA
[50] Institute of Space and Astronautical Science, JAXA, 3-1-1 Yoshinodai, Sagamihara, Kanagawa 229-8510, Japan
[51] Institució Catalana de Recerca i Estudis Avançats (ICREA), Barcelona, Spain
[52] Consorzio Interuniversitario per la Fisica Spaziale (CIFS), I-10133 Torino, Italy
[53] INAF, Osservatorio Astronomico di Torino, I-10025 Pino Torinese (TO), Italy
[54] Dipartimento di Fisica, Università di Roma "Tor Vergata," I-00133 Roma, Italy
[55] School of Pure and Applied Natural Sciences, University of Kalmar, SE-391 82 Kalmar, Sweden
Received 2009 December 11; accepted 2010 January 7; published 2010 January 28

ABSTRACT

The gamma-ray energy spectra of bright blazars of the LAT Bright AGN Sample (LBAS) are investigated using *Fermi*-LAT data. Spectral properties (hardness, curvature, and variability) established using a data set accumulated over 6 months of operation are presented and discussed for different blazar classes and subclasses: flat spectrum radio quasars (FSRQs), low-synchrotron peaked BLLacs (LSP-BLLacs), intermediate-synchrotron peaked BLLacs (ISP-BLLacs), and high-synchrotron peaked BLLacs (HSP-BLLacs). The distribution of photon index (Γ, obtained from a power-law fit above 100 MeV) is found to correlate strongly with blazar subclass. The change in spectral index from that averaged over the 6 months observing period is < 0.2–0.3 when the flux varies by about an order of magnitude, with a tendency toward harder spectra when the flux is brighter for FSRQs and LSP-BLLacs. A strong departure from a single power-law spectrum appears to be a common feature for FSRQs. This feature is also present for some high-luminosity LSP-BLLacs, and a small number of ISP-BLLacs. It is absent in all LBAS HSP-BLLacs. For 3C 454.3 and AO 0235+164, the two brightest FSRQ source and LSP-BLLac source, respectively, a broken power law (BPL) gives the most acceptable of power law, BPL, and curved forms. The consequences of these findings are discussed.

Key words: BL Lacertae objects: general – galaxies: active – galaxies: jets – gamma rays: general

Online-only material: color figures

1. INTRODUCTION

Launched into a low-Earth orbit on 2008 June 11, the *Fermi Gamma-Ray Space Telescope* continues providing excellent gamma-ray data for celestial sources. With significant improvement of sensitivity and bandpass over its predecessors (Atwood et al. 2009), the main instrument on *Fermi*—the Large Area Telescope (LAT)—enables detailed studies of time-resolved broadband gamma-ray spectra of a broad range of sources, including active galaxies. As discovered by EGRET on the Compton Observatory (Hartman et al. 1992; Fichtel et al. 1994), active galactic nuclei (AGNs) showing strong gamma-ray emission are associated with relativistic jets, whose presence was independently inferred from morphological and variability studies in other bands. The spectra of such objects in all observable bands are well described by broad power-law or curved distributions, indicating nonthermal emission mechanisms (Böttcher 2007). Very generally, the overall broadband spectral distributions of such jet-dominated AGNs, often called blazars have a two-humped shape, with the low-energy (IR–UV) hump attributed to synchrotron emission of energetic electrons radiating in magnetic field and the high-energy hump due to inverse Compton scattering by the same electrons (Ghisellini 1989; Dermer & Schlickeiser 1993; Sikora et al. 1994).

The first list of such AGNs detected by the *Fermi*-LAT, the LAT Bright AGN Sample (LBAS; Abdo et al. 2009f) includes bright, high Galactic latitude ($|b| > 10^{\circ}$) AGNs detected by the *Fermi*-LAT with high significance (Test Statistic, TS > 100) during the first 3 months of scientific operation. This sample comprises 58 Flat Spectrum Radio Quasars (FSRQs), 42 BLLac-type objects (BLLacs), two radio galaxies, and four quasars of unknown type. This somewhat conventional classification was based on the observed optical emission line equivalent widths and the Ca II break ratio (e.g., Marcha et al. 1996). Following the models used to describe the gamma-ray spectra obtained with previous gamma-ray observatories (e.g., Mattox et al. 1996), the early analysis reported in Abdo et al. (2009f) was carried out by fitting the gamma-ray spectra at energies above 200 MeV using a simple power-law (PL) model. This analysis revealed a fairly distinct spectral separation between FSRQs and BLLacs, with FSRQs having significantly softer spectra. The boundary photon index between the two classes was found to be $\Gamma \simeq 2.2$. It has been suggested (Ghisellini et al. 2009) that this separation results from different radiation cooling suffered by the electrons due to distinct accretion regimes in the two blazar classes.

While adopting such a simple spectral model was sufficient to investigate the source spectral hardness distribution, a PL model was clearly not the most appropriate choice for some bright sources which exhibited evident breaks or curvatures

[56] Royal Swedish Academy of Sciences Research Fellow, funded by a grant from the K. A. Wallenberg Foundation.
[57] Corresponding author: lott@cenbg.in2p3.fr
[58] Partially supported by the International Doctorate on Astroparticle Physics (IDAPP) program.

in their spectra. The departure of the functional form from a PL was investigated in some detail for the bright quasar 3C 454.3 (Abdo et al. 2009e), which underwent strong activity in the summer of 2008. The change of photon index $\Delta\Gamma$ was observed to be 1.2 ± 0.2, i.e., greater than the value of 0.5 expected from incomplete cooling of the emitting electrons. The observed break around 2.2 GeV was ascribed for mirroring a similar feature in the underlying emitting electron energy distribution; the Klein–Nishina effect was not ruled out, though the importance of photon–photon pair production requires the gamma-ray emission region to be close to the supermassive black hole. Clearly, understanding the details of the spectral break is important for understanding the structure and location of the dissipation region of jets in active galaxies.

The data first obtained with the EGRET instrument, now refined with *Fermi*, imply that the high Galactic latitude sky emits quasi-diffuse, uniform gamma-ray background (Sreekumar et al. 1998; Strong et al. 2004a; Abdo et al. 2009a). Its isotropy points to its extragalactic nature after subtraction of a quasi-isotropic gamma-ray emission component from cosmic ray electrons in an extended galactic halo. Most models account for at least a part of this background as originating from a large number of unresolved point sources, presumably jet-dominated AGNs. Here, the comparison of spectral properties of various classes of AGNs, integrated over their space density and luminosity, against the integral measurement of the unresolved component should provide additional clues regarding their contribution to the extragalactic diffuse background: can they make up the entire background, is another class of sources, e.g., star-forming galaxies (Fields et al. 2008) or is an additional truly diffuse component required? The issue is further complicated by the apparently different spectral forms of the luminous AGN associated with quasars as compared to the lineless BL Lac objects, as already hinted in Abdo et al. (2009f). It is thus important to determine whether the spectral feature seen in 3C 454.3 is common in all blazars and also whether it is connected to other blazar properties.

Here, we report on the detailed spectral analysis of bright LBAS sources using data accumulated over the first 6 months of the *Fermi*-LAT all-sky survey. In Section 2, we present the observations with the *Fermi*-LAT; Section 3 briefly discusses the classification scheme used in this paper. Section 4 contains the results regarding the photon index and observed deviations from a pure PL. The results and their consequences are discussed in Section 5.

2. OBSERVATIONS WITH THE LAT

The *Fermi*-LAT is a pair-conversion gamma-ray telescope sensitive to photon energies greater than 20 MeV. It is made of a tracker (composed of two sections, front and back, with different localization capabilities), a calorimeter, and an anticoincidence system to reject the charged-particle background. The LAT has a large peak effective area ($\sim 8000\,\mathrm{cm}^2$ for 1 GeV on-axis photons in the event class "diffuse" considered here), viewing ≈ 2.4 sr of the full sky with an angular resolution (68% containment angle) better than $\approx 1^\circ$ at $E = 1$ GeV (Atwood et al. 2009).

The data were collected from 2008 August 4 to 2009 February 1 in survey mode. To minimize systematics, only photons with energies greater than 100 MeV were considered in this analysis. In order to avoid contamination from Earth limb gamma rays, a selection on the zenith angle, $< 105^\circ$, was applied. The exposure was constant within 20% for all sources and amounted to about 1.5×10^6 m^{2}s at 1 GeV.

This analysis was performed with the standard analysis tool *gtlike*, part of the *Fermi*-LAT ScienceTools software package (version v9r12). The first set of instrument response functions (IRFs) tuned with the flight data, P6_V3_DIFFUSE, was used. In contrast to the preflight IRFs, these IRFs take into account corrections for pile-up effects. This correction being higher for lower energy photons, the measured photon index of a given source is about 0.1 higher (i.e., the spectrum is softer) with this IRF set as compared to the P6_V1_DIFFUSE one used previously in Abdo et al. (2009f). Photons were selected in circular regions of interest (ROI), 7° in radius, centered at the positions of the sources of interest. The isotropic background (the sum of residual instrumental background and extragalactic diffuse gamma-ray background) was modeled with a simple power law. The GALPROP model (Strong et al. 2004a, 2004b), version "gll_iem_v01.fit," was used for the galactic diffuse emission, with both flux and spectral photon index left free in the fit. All point sources with TS > 25 in the 6 month source list, lying within the ROI and a surrounding 5° wide annulus, were modeled in the fit with single power-law distributions. Different analyses were performed by fitting the spectra with various models over the whole energy range covered by the LAT above 100 MeV, or with a PL model over equispaced logarithmic energy bins (where the spectral index was kept constant and equal to the value fitted over the whole range). In the case of fits with broken power-law (BPL) models, the break energy (E_{Break}) bounding the ranges where different photon indices (Γ_1 and Γ_2) apply, could not be obtained directly from the fit for most sources because of convergence problem due the non-smooth character of the BPL function at the break energy. It was computed from a loglikelihood profile fitting procedure, with statistical uncertainties corresponding to a difference of $-2\Delta L = 1$ in the loglikelihood (L) with respect to its minimum. We refer the reader to D'Agostini (2004) regarding limitations with the use of asymmetric uncertainties.

The estimated systematic uncertainty on the flux is 10% at 100 MeV, 5% at 500 MeV, and 20% at 10 GeV. The energy resolution is better than 10% over the range of measured E_{Break}.

3. CLASSIFICATION

We employ the conventional definition of BL Lac objects outlined in Stocke et al. (1991); Urry & Padovani (1995); Marcha et al. (1996) in which the equivalent width of the strongest optical emission line is < 5 Å and the optical spectrum shows a Ca II H/K break ratio $C < 0.4$. BLLac sources were assigned to different subclasses (LSP-BLLacs, ISP-BLLacs and HSP-BLLacs standing for Low-, Intermediate-, and High-synchrotron peaked BLLacs, respectively) according to the position of their synchrotron peak, established from radio, optical, UV, and X-ray data: $\nu_{\mathrm{peak}} < 10^{14}$ Hz for LSP-BLLacs, 10^{14} Hz $< \nu_{\mathrm{peak}} < 10^{15}$ Hz for ISP-BLLacs and $\nu_{\mathrm{peak}} > 10^{15}$ Hz for HSP-BLLacs (Abdo et al. 2009b). Contemporaneous *Swift* data were used for a subset of 46 LBAS sources and archival ones for the others, as described in Abdo et al. (2009b).

4. RESULTS

4.1. Photon Index Distributions

Although some spectra display significant curvatures, the photon index obtained by fitting single power-paw models over the whole LAT energy range provides a convenient means to study the spectral hardness. Figure 1 displays the distributions

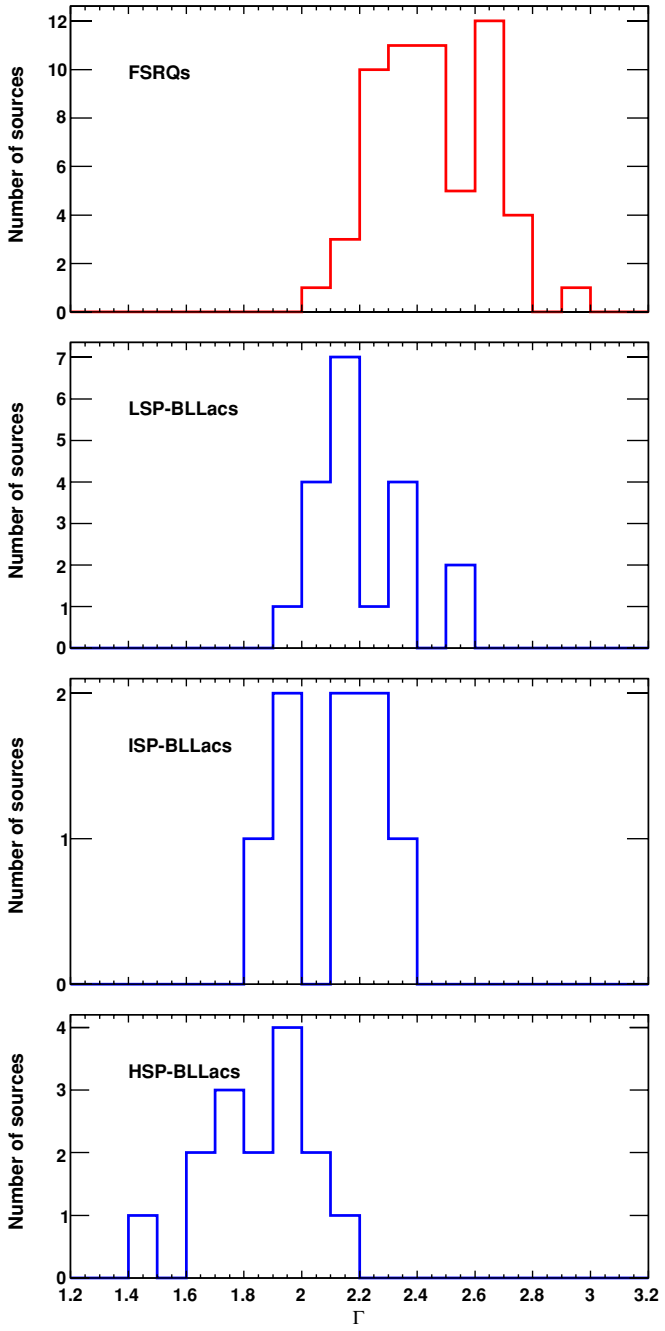

Figure 1. Gamma-ray photon index distributions for the four blazar subclasses.
(A color version of this figure is available in the online journal.)

of the resulting photon index for the four different subclasses. The remarkable separation between FRSQs and BLLacs already found in Abdo et al. (2009f) is of course still observed for spectra averaged over a 6 month (instead of 3 month) time span. Likewise, different BLLac subclasses are associated with distinct photon index distributions in the LAT range. The distributions have (mean, rms) = (2.46, 0.18) for FSRQs, (2.21, 0.16) for LSP-BLLacs, (2.13, 0.17) for ISP-BLLacs and (1.86, 0.17) for HSP-BLLacs. For comparison, the distributions given in Abdo et al. (2009f) had (mean, rms) = (2.40, 0.17), (1.99, 0.22) for FSRQs and BL Lacs, respectively. It must be kept in mind that the 6 month distributions have been obtained with an improved (more realistic) IRF set leading to a softer measured spectrum (Γ higher by ≃0.1 unit). Interestingly,

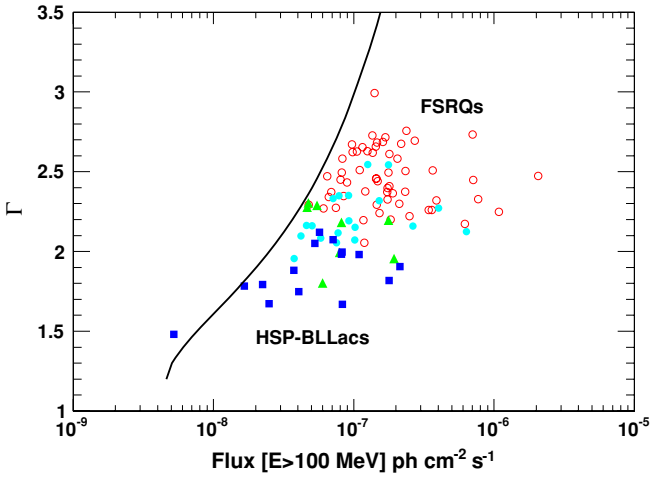

Figure 2. Photon index Γ vs. flux ($E > 100$ MeV) for the LBAS sources considered here. Open circles, red: FSRQs; solid symbols: BL Lacs (cyan circles: LSP-BLLacs, green triangles: ISP-BLLacs, blue squares: HSP-BLLacs). The solid curve represents the TS = 100 limit for a 3 months period (i.e., the defining condition of the LBAS sample) estimated for $(l, b) = (80°, 40°)$.
(A color version of this figure is available in the online journal.)

the largest difference (increase) in photon index between the 3 month and the 6 month data set is obtained for BL Lacertae (from $\Gamma = 2.24 \pm 0.12$ to $\Gamma = 2.54 \pm 0.07$), a BLLac intermittently exhibiting broad emission lines characteristic of FSRQs (Vermeulen et al. 1995). It would be interesting to investigate the correlation of this spectral evolution with properties in other bands.

The distributions in Figure 1 are remarkably narrow, with rms = 0.16–0.18, i.e., comparable to the index statistical uncertainties for the faintest LBAS sources. Note that the overlap between LSP-BLLac and FSRQ photon index distributions is small (LSP-BLLacs being harder), although both have similar positions of their synchrotron peaks. The gamma-ray photon index is thus a distinctive property of a blazar subclass. The low dispersion observed within a subclass strongly supports the idea that a very limited number of physical parameters (possibly only one), drive the spectrum shape in the GeV energy range. It can also be connected to distinct dominant emission mechanisms for the different classes, External Compton for the low-energy peaked sources and Synchrotron-Self Compton for the high-energy peaked ones, as discussed in Abdo et al. (2009b).

One must keep in mind that the LBAS sample, being significance limited (TS > 100 after 3 months of LAT operation) has an intrinsic bias such that faint sources can more easily be detected if they are hard. This situation is illustrated in Figure 2 (similar to Figure 7 in Abdo et al. 2009f), where the 6 month average photon index flux is plotted versus the corresponding flux for the four subclasses along with the approximate LBAS flux limit (for the first 3 months of operation). From this figure, the source subclass that appears potentially the most affected by this bias is that of HSP-BLLacs, which are substantially fainter than the other sources. However, as pointed out in Abdo et al. (2009b), more than 60% of known radio-loud HSP-BLLacs are included in the LBAS sample, so the measured photon index distribution is probably still representative of the full population.

4.2. Photon Index Variability

Given the narrowness of the photon index distribution for a given class, the photon index would not be expected to vary wildly over time for a given source. Two examples of weekly

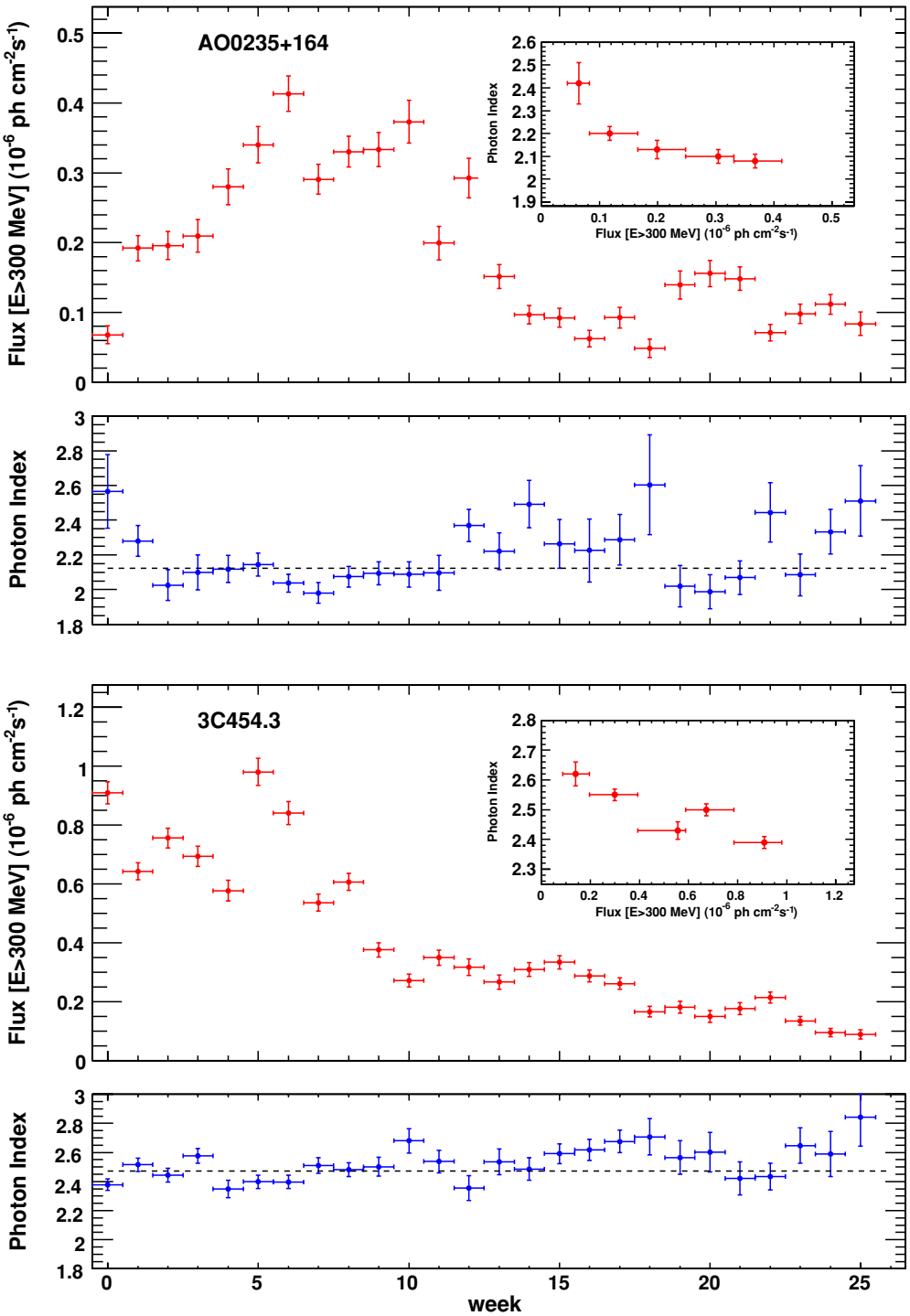

Figure 3. Measured weekly fluxes and photon index for 3C 454.3 and AO 0235+164 used as input of the simulations described in the text. The insets show the photon index resulting from an analysis where photons were sorted in five weekly flux bins plotted vs. the weekly flux.

(A color version of this figure is available in the online journal.)

flux and photon index light curves are shown in Figure 3 for the brightest FSRQ (3C 454.3) and LSP-BLLac (AO 0235+164) in the LBAS. The average photon index is shown as a dashed line in the corresponding panels. Although flux variations are large (flux variations by a factor >7) for both sources, the range of photon index values is only about 0.3 wide if one allows for a 1σ dispersion. The insets in Figure 3 display the photon index resulting from an analysis where photons were sorted in five bins in weekly flux, plotted versus the weekly flux. A weak "harder when brighter" effect can be seen for both sources.

To test the constancy of the photon index, the weekly photon indices were fitted with a constant model and the corresponding fractional excess variance (Vaughan et al. 2003) was calculated for the different LBAS sources, keeping only time periods where the sources were detected with a significance larger than 3σ. Figure 4, top, displays the distributions of normalized χ^2 values obtained for FSRQs (red), BLLacs (blue), and all sources (black). The means of these distributions are close to 1, as expected for a constant photon index, with no significant differences between FSRQs and BLLacs. For

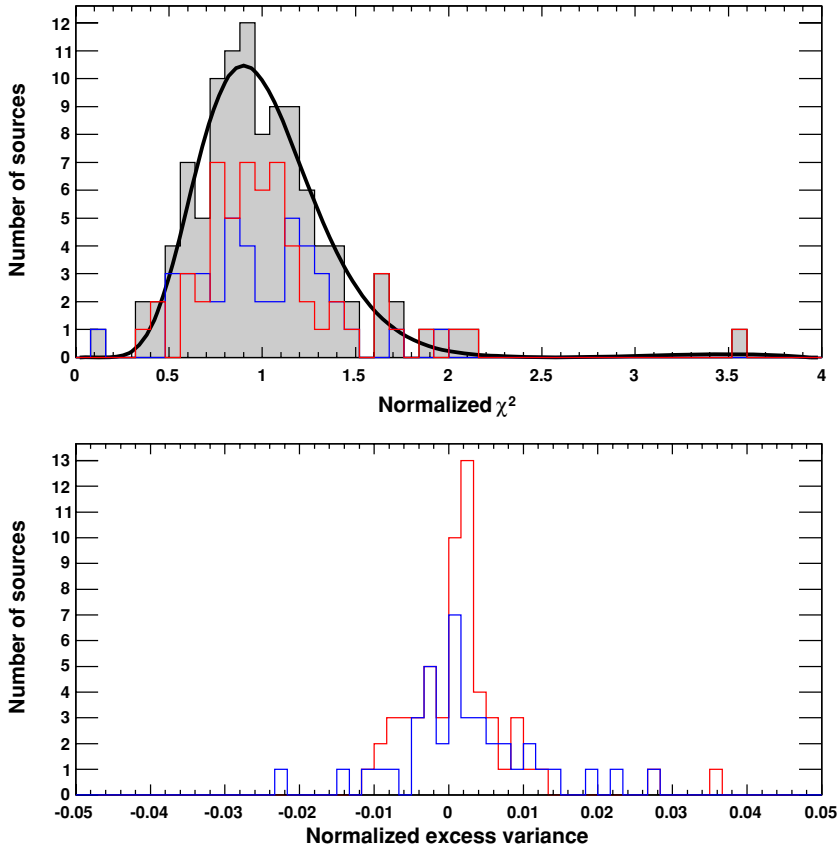

Figure 4. Top panel: normalized χ^2 distributions of the weekly photon indices for FSRQs (red), BLLacs (blue), and all sources (black). Bottom panel: normalized excess variance distributions of the weekly photon indices for FSRQs (red) and BLLacs (blue).

(A color version of this figure is available in the online journal.)

illustration, the normalized χ^2 distribution with 20 degrees of freedom (corresponding to an average source) expected in the case of a constant photon index is plotted as well. The source associated with a normalized χ^2 of 3.5 is PKS 1502+106 for which a clear indication of "harder when brighter" effect has been observed during a bright flare (Abdo et al. 2009c). Figure 4, bottom, shows the distributions of fractional excess variance for FSRQs and BLLacs. The means of the distributions are compatible with 0 (within 1σ); the same applies for all three BLLac subclasses. The widths of these distributions are in good agreement with the average statistical uncertainties (estimated from Equation (11) in Vaughan et al. 2003), i.e., 8×10^{-3} and 1.5×10^{-2} for FSRQs and BLLacs, respectively. Inspection of distributions of Pearson coefficients of the weekly flux versus photon index correlation does not reveal any strong trend for any subclass. The average variation of weekly photon index is plotted versus the relative flux (normalized to the average flux) in Figure 5 for the different blazar subclasses. The data from the eight brightest representatives of each subclass have been considered.[59] A weak "harder when brighter" effect is apparent in FSRQs, LSP-BLLacs and ISP-BLLacs, whereas no significant effect is present for HSP-BLLacs.[60]

These observations, aimed at determining the gross spectral features of a source ensemble, do not exclude fine spectral evolutions over short periods of time, e.g., regarding particular episodes of flaring activity, or for particular sources. They do, however, demonstrate that the photon index in the GeV range changes little with time and within a blazar subclass.

4.3. Spectra of Brightest Sources

In this section, we present the spectra obtained for the eight brightest representatives of the four subclasses, FSRQs (Figure 6), LSP-BLLacs (Figure 7), ISP-BLLacs (Figure 8), and HSP-BLLacs (Figure 9), ordered according to decreasing average flux. Upper limits are shown for bins associated with a TS lower than 9 (significance lower than 3σ) or with a number of source photons (predicted by the model) lower than 3. The brightest FSRQ, 3C 454.3 with an average flux ($E > 100$ MeV) of 2×10^{-6} ph cm^{-2} s^{-1}, exhibits a pronounced break around 2 GeV, as reported in Abdo et al. (2009e). Indications for breaks between 1 and 10 GeV are observed for essentially all of these FSRQ sources. This behavior is confirmed by comparing (Figure 10) the flux ($E > 2$ GeV) extrapolated from the spectral distribution in the range 100 MeV $< E < 2$ GeV, fitted with a power-law function, with the actual measured flux (obtained via a power-law fit in the $E > 2$ GeV energy range). For all sources considered, the measured flux is lower than the extrapolated flux by more than 30%. The spectral properties of these sources are summarized in Table 1, which also gives the difference in loglikelihood between the BPL and PL fits, the break energy in the source rest frame, $E'_{\rm Break} = E_{\rm Break} \times (1+z)$, and the source gamma-ray luminosity (computed as in Ghisellini et al. 2009). $E'_{\rm Break}$ lies between 1.6 and 10 GeV for all sources listed in

[59] A condition on the significance $> 1\sigma$, i.e., less restrictive than above, has been imposed in this analysis to minimize the effect of the instrumental bias against soft and faint states illustrated in Figure 2.

[60] The weak tendency toward softer spectra at high flux in HSP-BLLacs does not appear to be significant.

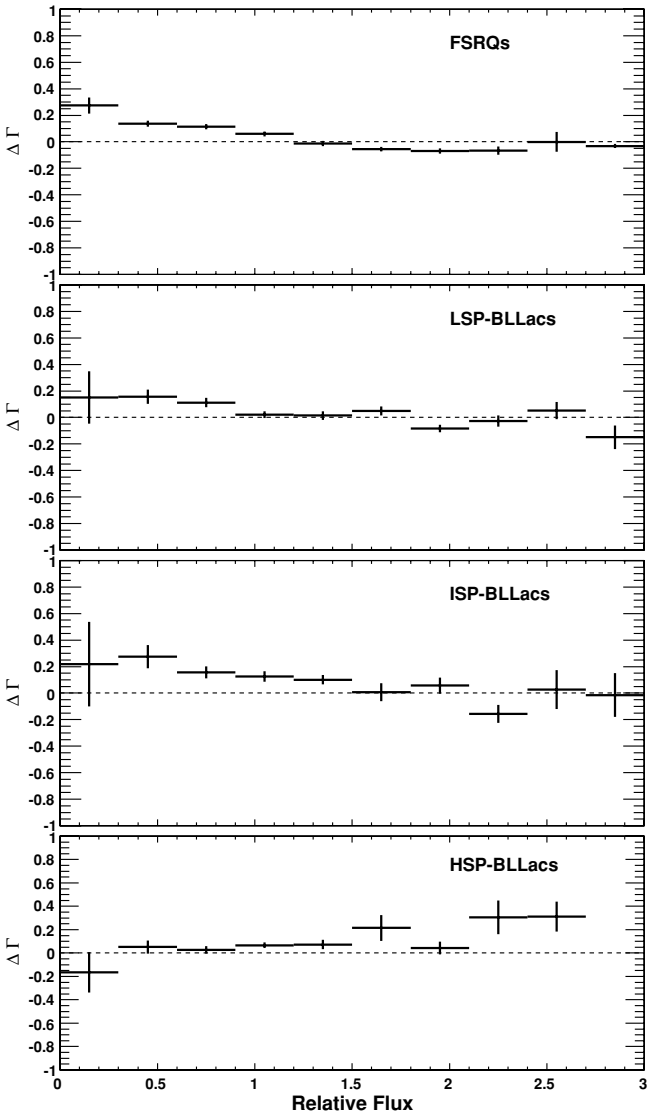

Figure 5. Average variation of photon index, Γ, vs. relative flux (normalized to the average flux), for the different blazar subclasses. The data are integrated over a weekly timescale, and only the eight brightest representatives of each subclass have been considered.

Table 1. No significant correlation is found between $E'_{\rm Break}$ and the gamma-ray luminosity (Figure 11).

The presence of a break is also clear for two of the brightest LSP-BLLacs (associated with the highest luminosities; Table 2) in the LBAS sample, AO 0235+164 and PKS 0537-441 (Figure 7), while it is less apparent for the fainter ones. From the inspection of these spectra, it can already be noted that the onset of the break, when present, seems to be located at higher energy than in the case of FSRQs while $E'_{\rm Break}$ lies in about the same range.

Some ISP-BLLacs (Figure 8) present clear signs of breaks (e.g., S5 0716+71 and S2 0109+22), while the rest, having in some cases very hard spectra, are compatible with power-law distributions up to several tens of GeV. Finally, no bright HSP-BLLac (Figure 9) shows any evidence for a break in the LAT energy range. This simple observation, which could be naively expected for sources many of which are detected at TeV energies, definitely rules out an instrumental effect as the origin of the break found for lower energy peaked sources. The indication for a moderate break in PKS 2155-304 (Aharonian et al. 2009) observed over a short time period (11 days) does not persist over a 6 month integration time.

For a small number of sources exhibiting the break, a few photons compatible with the source location are detected at high energy, at variance with the decreasing trend. Most of these have been cutoff by the condition on the minimum number of photons per bin (three). More statistics will be required to determine whether these photons do arise from these sources or just represent background fluctuations.

Figure 10 illustrates the general trend for the four subclasses. The trend observed in the presence of a spectral break (or curvature) parallels that observed in the photon index for the four different classes.

4.4. Spectra of Special Sources

For 19 of the 22 brightest LBAS FSRQs, a likelihood ratio test (LRT; Mattox et al. 1996) rejects the hypothesis that the spectrum is a PL (null hypothesis) against the one that the spectrum is a BPL, at a confidence level greater than 97%. The four top panels of Figure 12 show spectra of representative sources where the break is clear. The spectral properties of these sources (PL and BPL fit results, difference in loglikelihood between the two fits) are reported in Table 1 as well. The two bottom left panels correspond to two of the three sources having the confidence level less than 97% (the other being PKS 2022-07, whose spectrum is given in Figure 6). For these two sources, a break located around 10 GeV cannot be excluded.

The last two panels of Figure 12 present the energy spectra of sources of particular interest, Mrk 501 and 1ES 0502+675. Mrk 501, the archetypal example of an extreme HSP-BLLac, is hard ($\Gamma = 1.75 \pm 0.06$) and does not exhibit any sign of curvature, in keeping with the behavior of the other HSP-BLLacs. The other one corresponds to 1ES 0502+675, an HSP-BLLac which exhibits an unusual concave energy spectrum ($\Gamma_1 = 2.68 \pm 0.18$, $\Gamma_2 = 1.47 \pm 0.10$, $E_{\rm break} = 1.4 \pm 0.6$ GeV). The LRT indicates that a BPL model is favored against a PL with a significance level of 2×10^{-4}. The very hard spectrum above 1.4 GeV would make this source a prime target for TeV observations although the redshift is fairly large (0.416).

4.5. Detailed Analysis of 3C 454.3 and AO 0235+164 Energy Spectra

The data accumulated over 6 months enable us to discriminate between different spectral models for the two brightest sources with spectra exhibiting strong departure from a pure PL, namely 3C 454.3 and AO 0235+164. Figure 13 shows the results of fits with different models: PL (thin lines), BPL (thick solid), and log-parabola (dashed) are compared with the data. Surprisingly, a BPL model is favored as the best fit for both sources. Despite the good statistics, no curvature is apparent in the energy range below the break. The fitted parameters are: $F[E > 100\ {\rm MeV}] = (1.97 \pm 0.03) \times 10^{-6}$ ph cm^{-2} s^{-1}, $\Gamma_1 = 2.39 \pm 0.02$, $\Gamma_2 = 3.42 \pm 0.11$, $E_{\rm break} = 2.5 \pm 0.3$ GeV for 3C 454.3 and $F[E > 100\ {\rm MeV}] = (0.60 \pm 0.02) \times 10^{-6}$ ph cm^{-2} s^{-1}, $\Gamma_1 = 2.05 \pm 0.02$, $\Gamma_2 = 2.95 \pm 0.16$, $E_{\rm break} = 4.5^{+1.5}_{-1.0}$ GeV for AO 0235+164. While the break energy is somewhat larger for AO 0235+164 than for 3C 454.3, the photon index change ($\Gamma_2 - \Gamma_1$) is about the same (0.90 ± 0.16 versus 1.03 ± 0.11). The similarity of the break feature for two sources belonging to different subclasses, FSRQ and LSP-BLLac, with different line strengths, seems to rule out any absorption effect in the LSP-BLLacs.

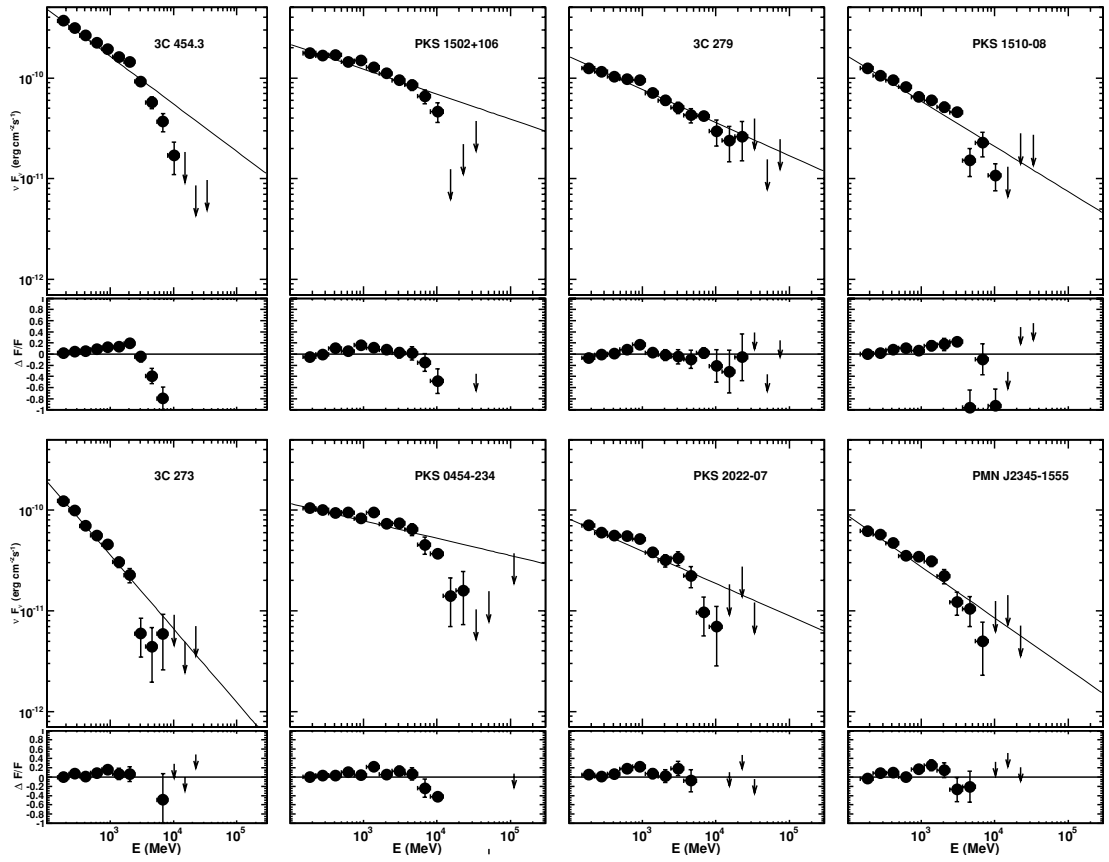

Figure 6. Gamma-ray spectra of the eight brightest FSRQs in the LBAS sample obtained for equispaced logarithmic bins (dots), together with residues with respect to the fitted power-law model (solid lines in upper panels).

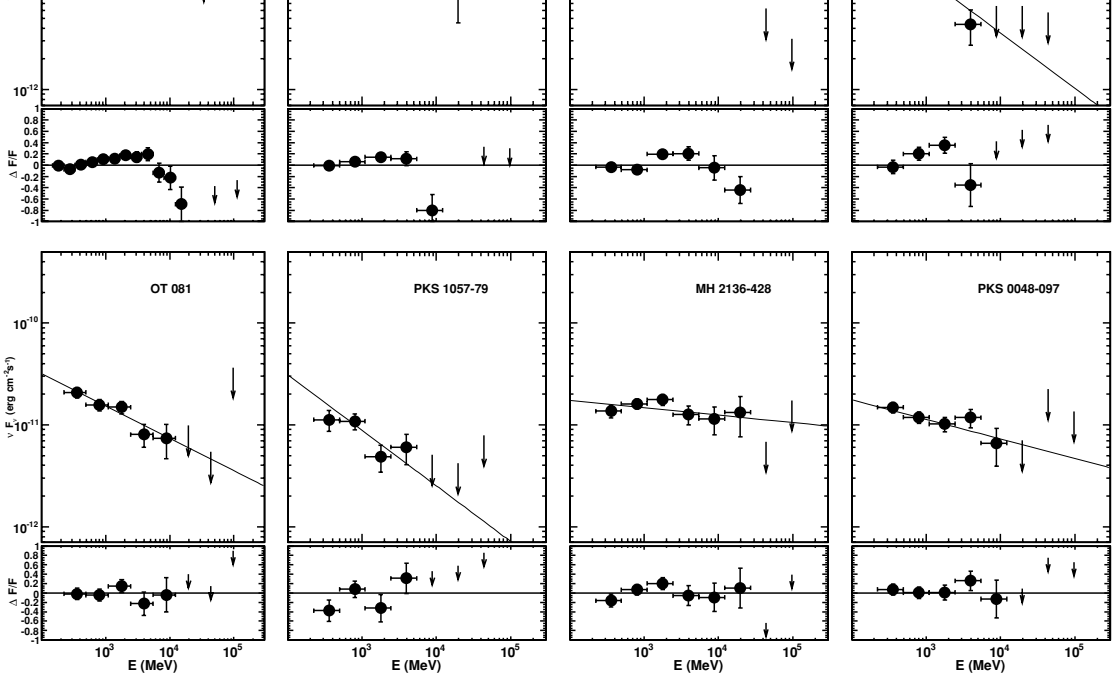

Figure 7. Same as Figure 6, but for the eight brightest LSP-BLLacs in the LBAS sample.

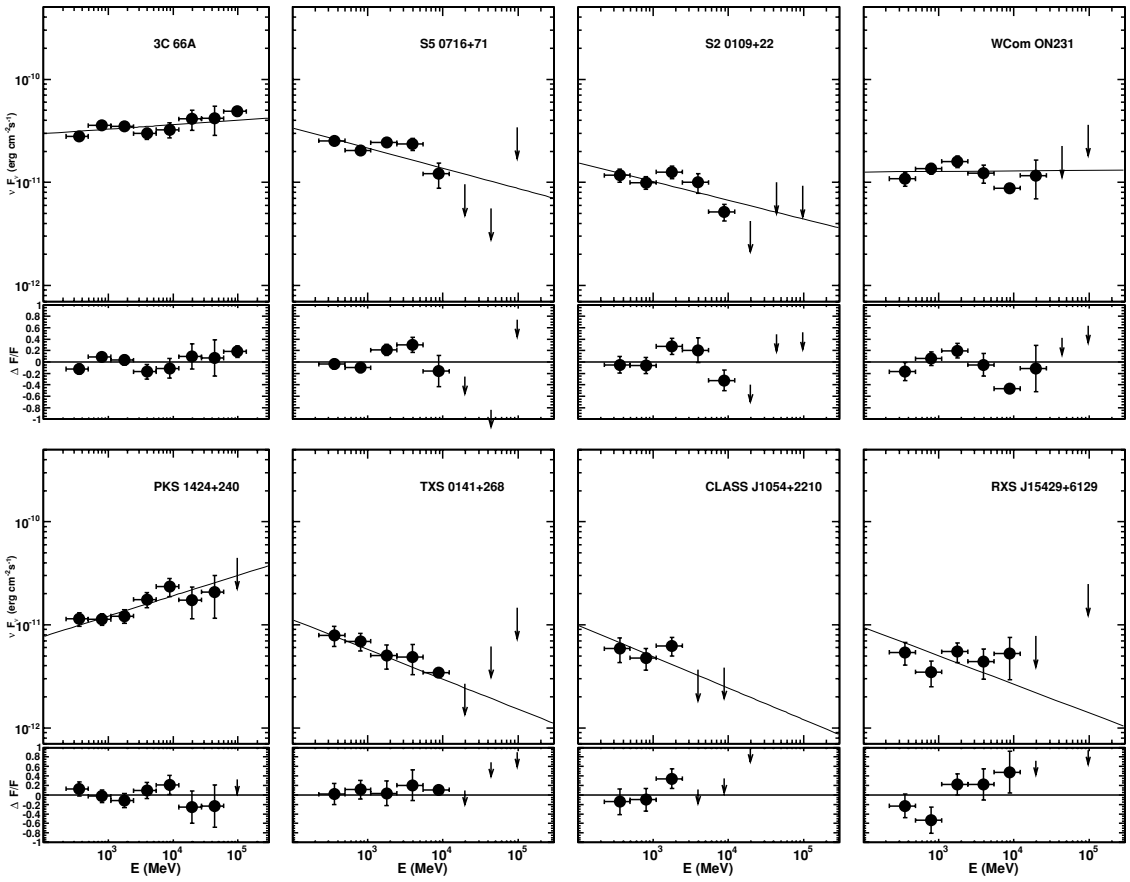

Figure 8. Same as Figure 6, but for the eight brightest ISP-BLLacs in the LBAS sample.

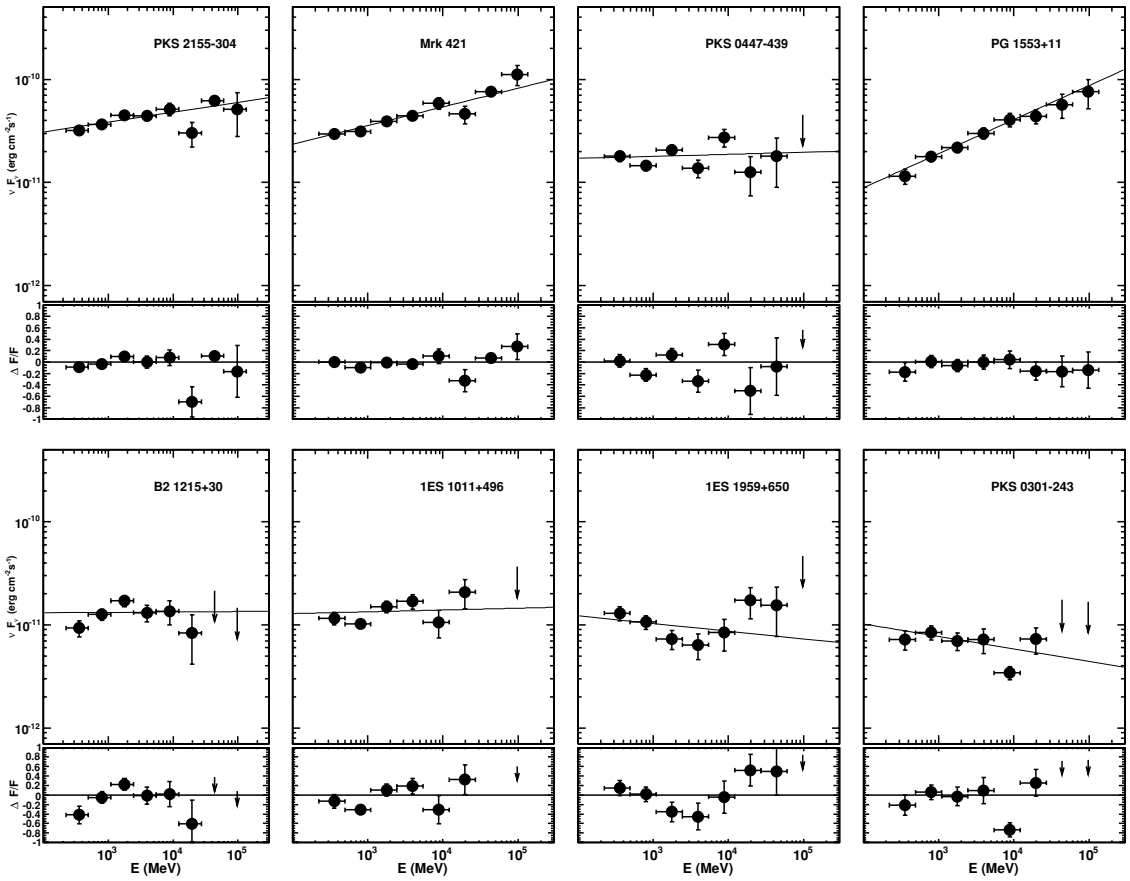

Figure 9. Same as Figure 6, but for the eight brightest HSP-BLLacs in the LBAS sample.

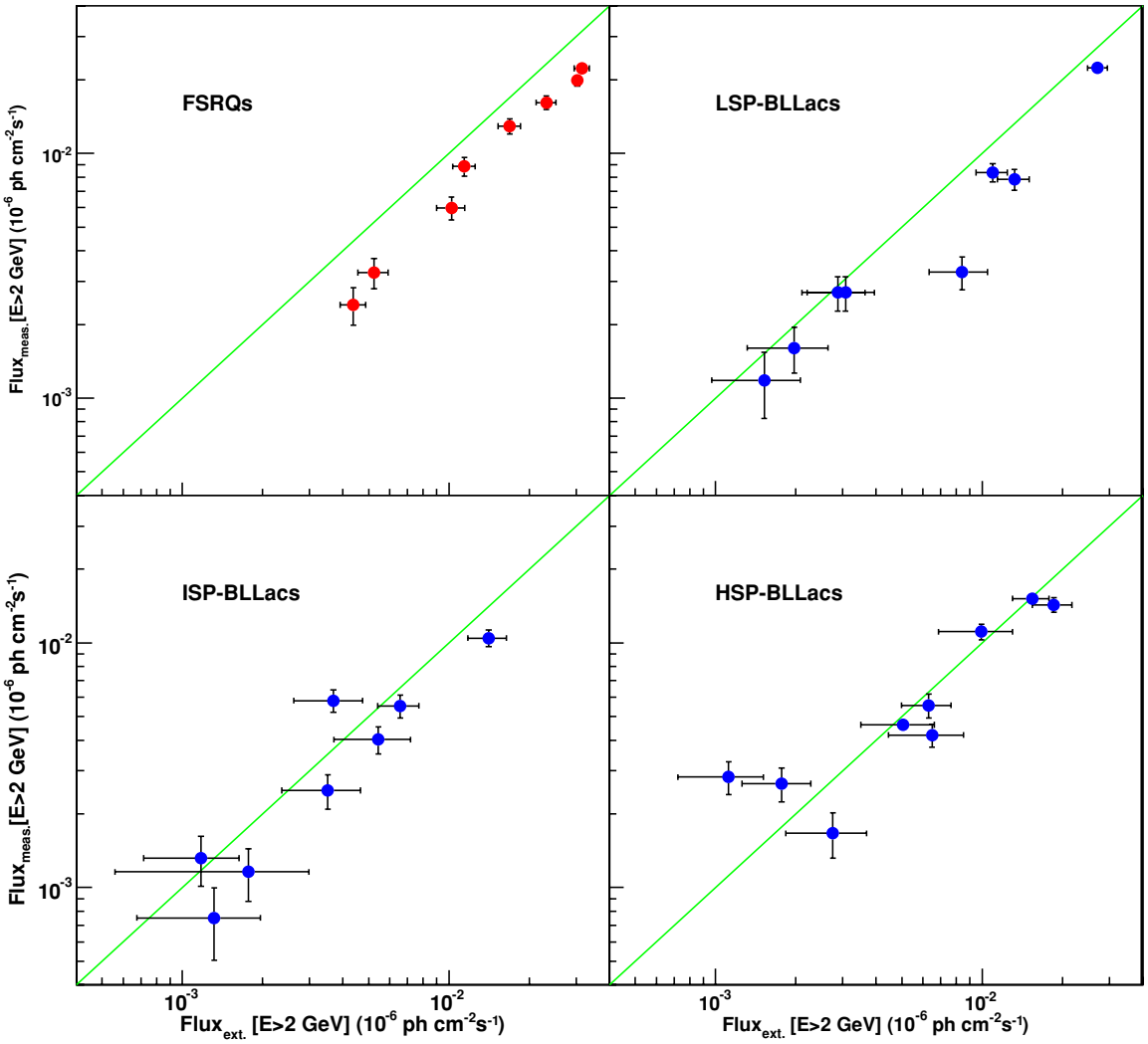

Figure 10. Measured vs. extrapolated flux above 2 GeV for the eight brightest sources of each blazar subclass. The distance of the points from the diagonal is indicative of the presence of a spectral break.

(A color version of this figure is available in the online journal.)

4.6. Apparent Curvature Due to Varying Spectral Hardness

An energy spectrum with time varying hardness may exhibit an apparent curvature when integrated over an extended period of time. To assess the magnitude of this effect, both analytical estimates and simulations assuming pure power-law distributions with flux and photon index corresponding to those actually measured over weekly time bins have been performed. Figure 3 shows the 3C 454.3 and AO 0235+164 weekly light curves and corresponding photon index. With these input data, the calculated spectra (assuming constant exposure) are not found to exhibit significant curvatures (Figure 14). Figure 15 compares the simulated photon count distribution obtained within the 90% containment radius around the source (blue) with the data (black). The effect of spectral hardness varying with time clearly cannot alone account for the observed features.

5. DISCUSSION

The trend in the observed gamma-ray photon index reported here confirms that reported earlier using 3 months of data: FSRQs, with a gamma-ray photon index greater than 2, are softer than BLLacs, indicating that the peak of the high-energy component in FSRQS is always lower than 100 MeV. For BLLacs, the gamma-ray photon index correlates with the different BLLac subclasses, which themselves are defined by the position of the synchrotron peak. The measured photon index shifts from $\Gamma > 2$ to $\Gamma < 2$, indicating that the peak energy of the high-energy component of the spectral energy distribution (SED) sweeps across the *Fermi* energy range from LSP-BLLacs to HSP-BLLacs.

The photon index being related to the shape of the emitting electron energy distributions, different regions of the electron distributions (from the high- to the low-energy ends for FSRQs/LSP-BLLacs and HSP-BLLacs, respectively) are probed in the LAT range. One would thus expect different spectral variability patterns in the LAT energy range for different blazar classes.

Using weekly light curves obtained over the first 6 months of LAT operation, this expectation does not seem to be corroborated by the data. The gamma-ray photon index appears remarkably stable with time, irrespective of the blazar class. This feature is in line with the observed narrowness of the index distribution for a class: a strongly varying photon index for a source would inevitably lead to a broad class distribution as different

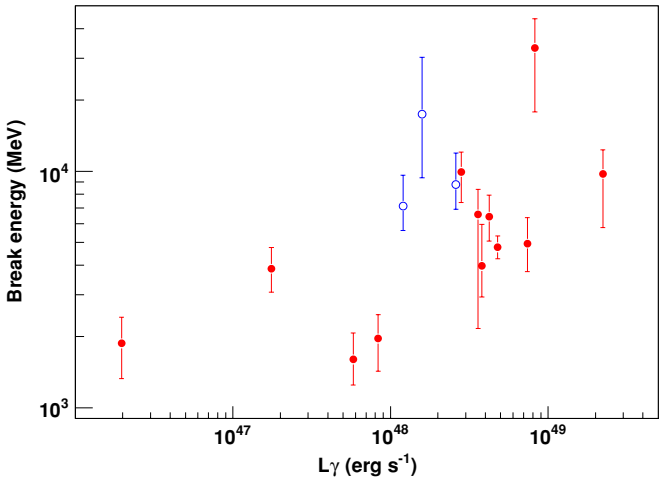

Figure 11. Break energy vs. gamma-ray luminosity for the FSRQs (closed red symbols) and LSP-BLLacs (open blue symbols) listed in Tables 1 and 2, respectively.

(A color version of this figure is available in the online journal.)

sources would be "caught" in different states. This apparent constancy of the photon index for all blazar classes may appear surprising, since for different classes, different electron energies (potentially associated with different cooling timescales, $t_{\rm cool}$) emit gamma rays in the LAT energy range. However, estimates of the cooling time show that within one week, all pairs with Lorentz factors $\gamma > 5/\delta_{10}u'$ have cooled down (where δ_{10} is the Doppler factor $\delta/(1+z)$ divided by 10, and u' is the jet frame energy density in erg cm^{-3} of the ambient magnetic field, or photon field provided scattering occurs in the Thomson regime). For sufficiently large u', the LAT energy range falls in the complete cooling regime. Spectral hysteresis may then be expected on timescales shorter than weekly if the duration of electron injection is sufficiently limited $\ll t_{\rm cool}$. Flux variations on weekly timescales may then reflect a varying injected energy content into the emission region from one week to another. Alternatively, continuous particle injection on at least weeks timescale could stabilize the spectral index. In the case of lower u', constant spectral indices can still be expected during flux variations in the LAT energy range if continuous particle injection is maintained for a time range significantly longer than the cooling time of the gamma-ray emitting particles (e.g., Kirk & Mastichiadis 1999). Flux changes then constrain the duration of particle injection. As more data are accumulated, possible exceptions to the observed index stability may appear. However, we can safely claim that a very soft spectrum for an HSP-BLLac, like that reported from EGRET for PKS 2155-304, $\Gamma = 2.35$ (Hartman et al. 1999), or a very hard one for a FSRQ, like the

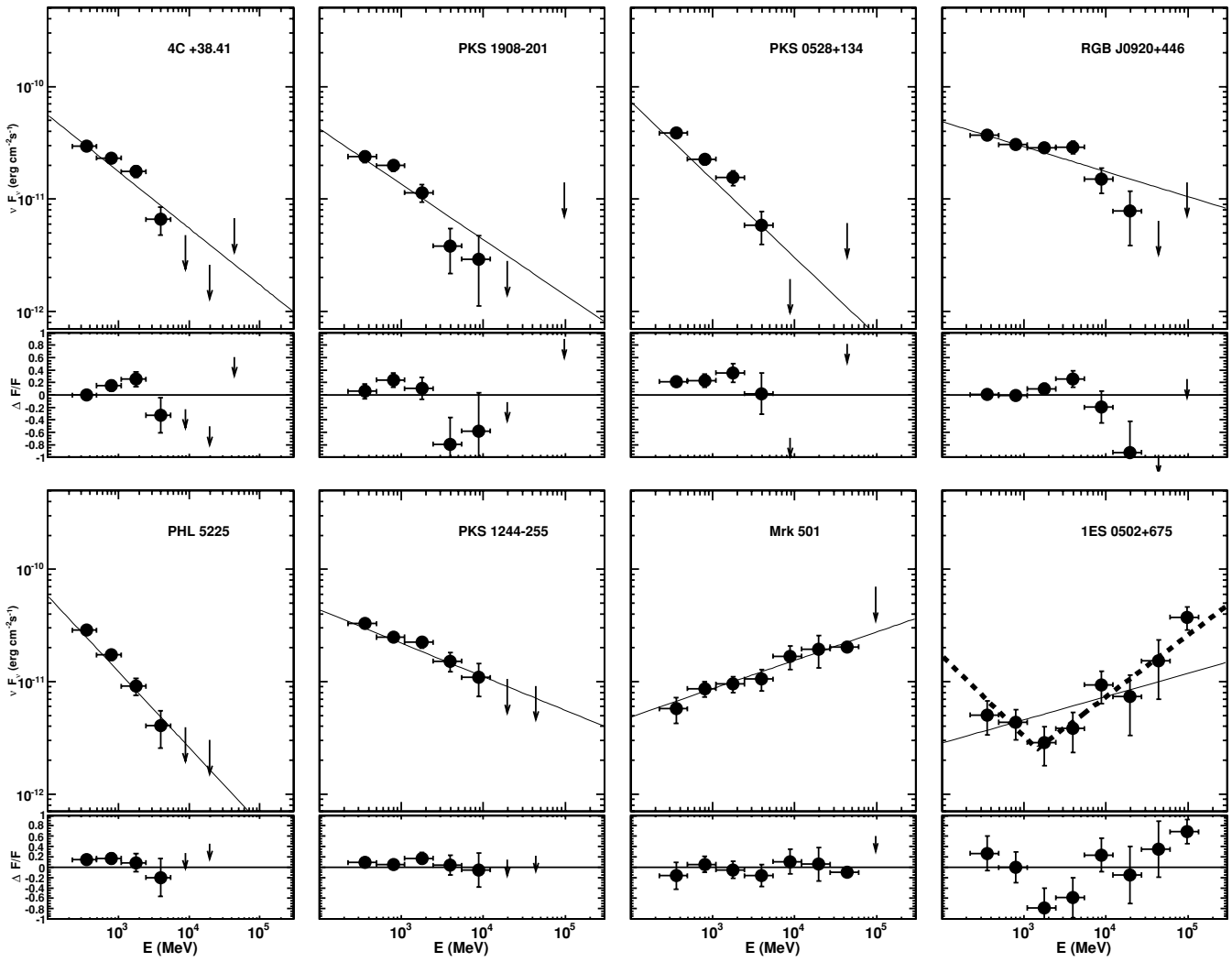

Figure 12. Same as Figure 6, but for eight particular sources in the LBAS sample.

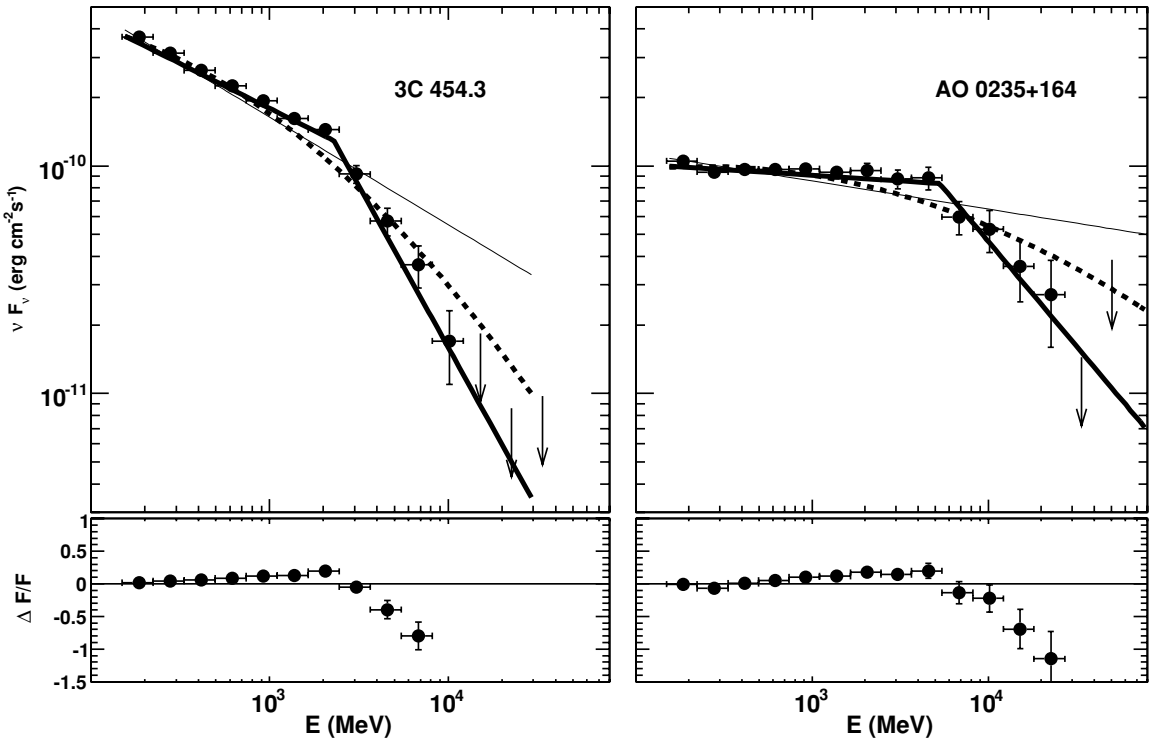

Figure 13. Upper panels: energy spectra of 3C 454.3 (left panel) and AO 0235+164 (right panel) compared with fit results obtained with different models: PL (thin solid), BPL (thick solid), and log-parabola (dashed).

one reported from *AGILE* for 3C 454.3, $\Gamma = 1.7$ (Vercellone et al. 2009), represent very rare occurrences.

All blazar spectra measured by EGRET were represented with pure PL. Thanks to its improved sensitivity, *Fermi* has revealed that the spectra of some low-energy peaked blazars display strong departure from a pure-PL behavior, with a BPL function as the best model. This feature being present for essentially all FSRQs where it can be detected with sufficient significance, it is likely to be a general character of this class. The three brightest LSP-BLLacs, in which this effect is also clearly seen, have higher luminosity ($L_\gamma > 10^{47}$ erg s^{-1}) than the rest of the LBAS LSP-BLLacs. Two of them are known to exhibit broad emission lines in low emission states, so could be FSRQs whose lines are hidden by nonthermal emission in active states. As discussed in Abdo et al. (2009e), the difference in photon index for most sources is significantly larger than 0.5 expected for an incomplete cooling effect. An absorption effect seems to be ruled out as well, since to produce a break in the 1–10 GeV, the photon field should have an energy peaking in the 0.05–0.5 KeV range, which excludes the broad-line region peaking in the UV. This feature most likely reflects the energy distribution of the emitting electrons. For the low-energy peaked sources where it is seen, Γ is greater than 2, i.e., the LAT range corresponds to "the falling edge" of the IC hump, where the highest energy electrons contribute. This feature could indicate a cutoff in that distribution, possibly related to limitations in the acceleration process (e.g., Drury 1991; Webb et al. 1984). Comparison of the maximum electron energies determined by the SED for PKS 2155-304, an HSP-BLLac where a one-zone synchrotron/SSC model was applied to derive the magnetic field and Doppler factor, showed that such an interpretation requires that the acceleration rate be approximately 3 orders of magnitude smaller than the maximum acceleration rate determined by the Larmor timescale (Finke et al. 2008). A Klein–Nishina break, expected in the context of a dominating External Compton emission process where the electrons upscatter BLR photons, is predicted to set in around $\frac{15\delta}{\Gamma(1+z)}$ GeV, where Γ is the blob bulk Lorentz factor (Ghisellini & Tavecchio 2009), i.e., significantly higher than the energies found here.

Irrespective of its origin, this feature, common for FSRQs and some LSP-BLLacs, has important practical consequences. First, it surely complicates the assessment of extragalactic background light (EBL) attenuation effects using FSRQs and LSP-BLLacs, as fewer photons are detected in the >10 GeV energy range. Second, as the low-energy peaked blazars are likely to represent the bulk of the blazar population, this break must manifest itself in (and be considered when evaluating) the contribution of unresolved blazars to the extragalactic diffuse γ-ray background. Finally, this effect must be considered when estimating the detectability of a source in the TeV range.

The concave shaped SED measured for the X-ray selected object 1ES 0502+675 ($z = 0.416$) opens interesting questions. It could potentially be a spurious feature resulting from the spatial confusion of a hard source with a soft one. No evidence for a second source has been found using the *gttsmap* tool of the standard ScienceTools package. The closest CRATES source is 1.°5 away. If confirmed, this peculiar spectral shape indicates either two components (e.g., Synchrotron-Self Compton and External Compton in the context of leptonic models) in the high-energy SED (however not expected in HSP-BLLacs in the framework of one-zone leptonic models), or the turnover from the synchrotron to the high-energy component, although the contemporaneous SEDs (Abdo et al. 2009b) obtained during that period does not seem to support that interpretation. This object should be a prime target for TeV instruments, opening interesting perspectives for studies on EBL absorption at TeV energies given its redshift.

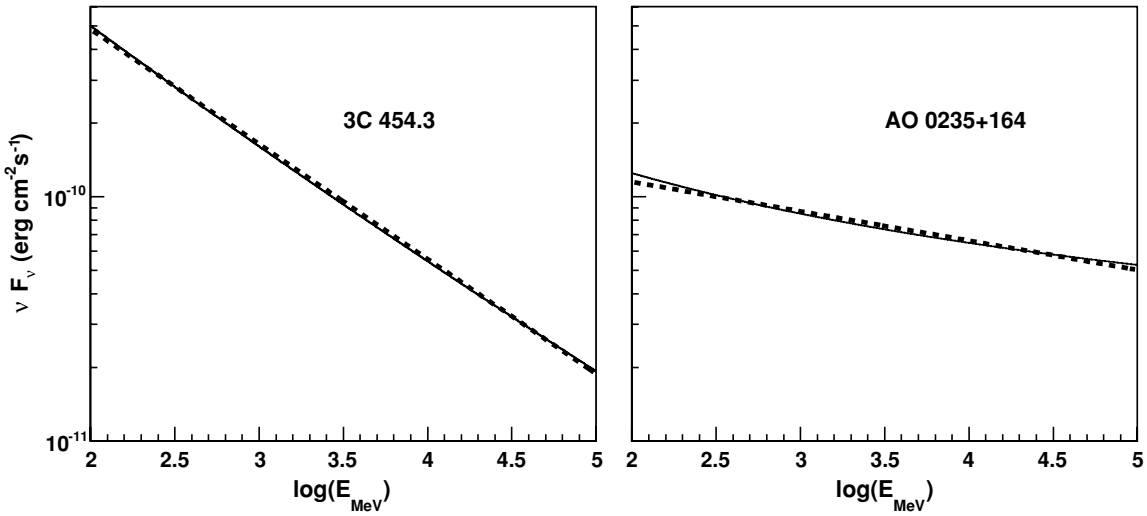

Figure 14. Analytical energy spectra (solid curves) of 3C 454.3 and AO 0235+164 resulting from summing power-law distributions with parameters (flux, photon index) as measured in weekly bins (Figure 4). The dashed lines represent PL fits.

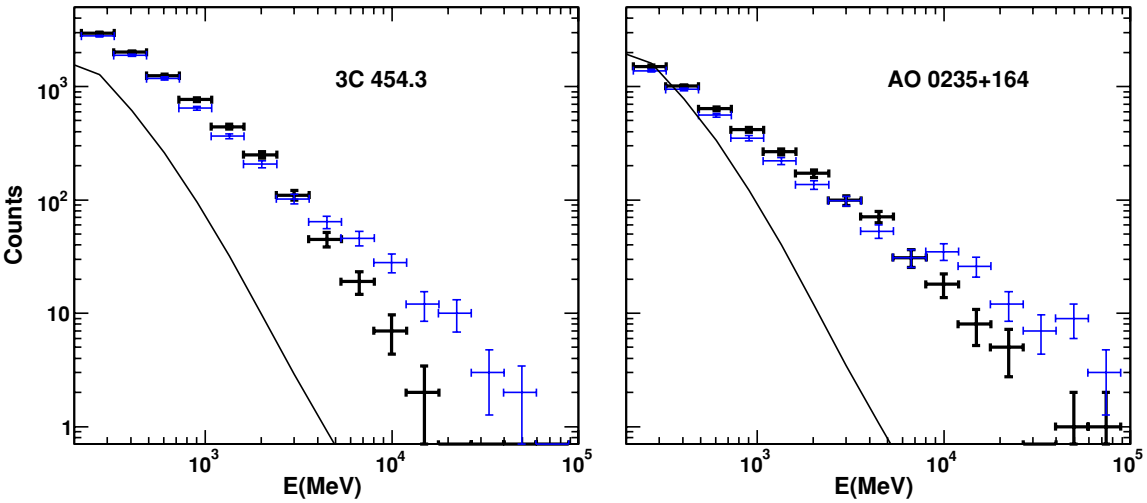

Figure 15. Count distributions within the 90% containment radius of simulated (blue and thin) and real (black and thick) data for 3C 454.3 and AO 0235+164. The solid curve corresponds to the total contribution of galactic and isotropic diffuse backgrounds.

(A color version of this figure is available in the online journal.)

A similar behavior, although less significant, has also been found for 1ES 1959+650 (Figure 8) and PG 1246+586, which is not included in the LBAS sample but is present in the LAT Bright Source List[61] (Abdo et al. 2009d). The spectra of other sources (e.g., W Comae) exhibit a wavy shape possibly indicative of multiple components as mentioned above. More detailed analysis will be necessary to resolve this issue.

6. CONCLUSION

The spectral properties of the LBAS blazars in the gamma-ray band, as determined over the first 6 months of LAT operation, have been presented. The average photon index of LBAS blazars are found to be $\Gamma = 2.46$ for FSRQs, $\Gamma = 2.21$ for LSP-BLLacs, $\Gamma = 2.13$ for ISP-BLLacs and $\Gamma = 1.86$ for HSP-BLLacs, with an rms of 0.16–0.18. Spectral breaks have been observed to be common features in FSRQs (the break energy ranging from 1 to 10 GeV in the source frame for the brightest sources), and present also in some bright LSP-BLLacs. The different spectral features reported here represent challenges for theoretical models aiming at describing the blazar phenomenon. Although the fairly strong correlation between photon index and blazar class fits well within pictures (Ghisellini et al. 1998; Böttcher & Dermer 2002) where the cooling due to strong ambient radiation fields (manifesting themselves via the presence of emission lines) limits the acceleration of particles at high energy, the near constancy of this photon index with time and flux variation provides new constraints on the emitting particle dynamics. Moreover, the fact that spectra for most FSRQs and some LSP-BLLacs are best modeled by a BPL with a break in the 1–10 GeV range is quite unexpected, the break representing a distinctive feature of these sources. The LAT has already revealed novel aspects of gamma-ray blazars and will help refine the new picture that progressively emerges as more data (both in the gamma-ray and other bands) are accumulated.

The *Fermi* LAT Collaboration acknowledges generous ongoing support from a number of agencies and institutes that have supported both the development and the operation of the LAT as well as scientific data analysis. These include the National

[61] The low confidence association obtained with 3 months worth of data has by now turned into a high-confidence one for this source.

Table 1
Spectral Properties of Selected FSRQs

Name	l	b	$\mathrm{Flux_{PL}}$[a]	Γ	ΔL	$\mathrm{Flux_{BPL}}$[a]	Γ_1	Γ_2	$\Delta\Gamma$	E_{Break} (GeV)	z	E'_{Break} (GeV)	Luminosity[b]
3C 454.3	86.12	−38.1	2.053 ± 0.02	2.47 ± 0.01	−54.7	1.994 ± 0.029	2.40 ± 0.01	3.51 ± 0.12	1.10 ± 0.12	$2.5^{+0.3}_{-0.3}$	0.859	$4.8^{+0.55}_{-0.55}$	44.1
PKS 1502+106	11.37	54.58	1.068 ± 0.02	2.24 ± 0.01	−34.0	1.024 ± 0.019	2.17 ± 0.01	3.06 ± 0.12	0.89 ± 0.12	$3.45^{+0.9}_{-0.15}$	1.839	$9.7^{+2.6}_{-0.4}$	185
3C 279	305.1	57.06	0.754 ± 0.01	2.32 ± 0.02	−6.60	0.724 ± 0.021	2.24 ± 0.03	2.50 ± 0.05	0.25 ± 0.06	$1.05^{+0.3}_{-0.2}$	0.536	$1.6^{+0.5}_{-0.3}$	5.0
PKS 1510−08	351.2	40.13	0.739 ± 0.02	2.47 ± 0.02	−7.13	0.717 ± 0.042	2.42 ± 0.05	3.08 ± 0.25	0.66 ± 0.26	$2.8^{+0.7}_{-0.6}$	0.36	$3.9^{+0.9}_{-0.8}$	1.60
3C 273	289.9	64.36	0.682 ± 0.02	2.73 ± 0.03	−9.12	0.669 ± 0.023	2.68 ± 0.03	3.66 ± 0.28	0.97 ± 0.28	$1.6^{+0.5}_{-0.5}$	0.158	$1.9^{+0.55}_{-0.55}$	0.19
PKS 0454−234	223.7	−34.9	0.632 ± 0.01	2.19 ± 0.01	−23.5	0.604 ± 0.016	2.11 ± 0.02	3.28 ± 0.21	1.16 ± 0.21	$4.95^{+1.1}_{-0.13}$	1.003	$9.95^{+2.1}_{-0.25}$	22.1
PKS 2022−07	36.89	−24.3	0.439 ± 0.01	2.38 ± 0.03	−4.54	0.420 ± 0.018	2.32 ± 0.03	2.84 ± 0.17	0.52 ± 0.18	$2.75^{+0.8}_{-0.18}$	1.388	$6.6^{+1.8}_{-0.45}$	31.1
TXS 1520+319	50.14	57.04	0.381 ± 0.01	2.52 ± 0.03	−3.95	0.364 ± 0.016	2.45 ± 0.04	2.90 ± 0.15	0.45 ± 0.16	$1.6^{+0.8}_{-0.4}$	1.487	$4.0^{+2.0}_{-0.1}$	35.4
4C +38.41	61.08	42.40	0.229 ± 0.01	2.50 ± 0.04	−10.1	0.211 ± 0.014	2.36 ± 0.05	4.06 ± 0.50	1.70 ± 0.50	$2.3^{+0.55}_{-0.5}$	1.814	$6.4^{+1.5}_{-0.15}$	39.3
PKS 1908−201	16.89	−13.1	0.160 ± 0.01	2.42 ± 0.06	−9.31	0.143 ± 0.018	2.09 ± 0.13	3.18 ± 0.22	1.09 ± 0.25	$0.9^{+0.25}_{-0.25}$	1.119	$1.95^{+0.55}_{-0.55}$	7.75
PKS 0528+134	191.3	−11.0	0.309 ± 0.02	2.72 ± 0.05	−7.42	0.268 ± 0.020	2.52 ± 0.07	3.87 ± 0.47	1.34 ± 0.48	$1.6^{+0.45}_{-0.4}$	2.07	$4.9^{+1.4}_{-1.2}$	71.4
RGB J0920+446	175.7	44.82	0.247 ± 0.01	2.22 ± 0.03	−7.61	0.235 ± 0.012	2.16 ± 0.03	4.86 ± 0.84	2.70 ± 0.84	$1.0^{+3.0}_{-0.5}$	2.19	$3.3^{+11.0}_{-1.5}$	67.2

Notes.
[a] 10^{-6} ph $[E > 100\ \mathrm{MeV}]\ \mathrm{cm^{-2}\ s^{-1}}$.
[b] 10^{47} erg $\mathrm{s^{-1}}$.

Table 2
Spectral Properties of Selected BLLacs

Name	l	b	$\mathrm{Flux_{PL}}$[a]	Γ	ΔL	$\mathrm{Flux_{BPL}}$[a]	Γ_1	Γ_2	$\Delta\Gamma$	E_{Break} (GeV)	z	E'_{Break} (GeV)	Luminosity[b]
LSP-BLLacs													
AO 0235+164	156.7	−39.0	0.630 ± 0.01	2.12 ± 0.01	−20.8	0.599 ± 0.016	2.04 ± 0.02	2.80 ± 0.12	0.75 ± 0.13	$4.5^{+1.5}_{-1.0}$	0.94	$8.8^{+3.0}_{-1.9}$	19.6
PKS 0537−441	250.0	−31.0	0.400 ± 0.01	2.28 ± 0.02	−8.51	0.380 ± 0.015	2.20 ± 0.03	3.08 ± 0.23	0.87 ± 0.24	$3.8^{+1.3}_{-0.8}$	0.892	$7.1^{+2.5}_{-1.5}$	10.1
PKS 0426−380	240.7	−43.6	0.274 ± 0.01	2.18 ± 0.03	−7.17	0.255 ± 0.012	2.10 ± 0.03	3.36 ± 0.45	1.26 ± 0.45	$8.3^{+6.0}_{-0.4}$	1.112	$17.5^{+13.0}_{-0.8}$	12.3
HSP-BLLac													
1ES 0502+675	143.7	15.89	0.019 ± 0.00	1.70 ± 0.14	−8.40	0.064 ± 0.015	2.68 ± 0.18	1.47 ± 0.10	-1.2 ± 0.21	$1.4^{+0.7}_{-0.5}$	0.416	$2.0^{+1.0}_{-0.7}$	0.12

Notes.
[a] 10^{-6} ph$[E > 100\ \mathrm{MeV}]\ \mathrm{cm^{-2}\ s^{-1}}$.
[b] 10^{47} erg $\mathrm{s^{-1}}$.

Aeronautics and Space Administration and the Department of Energy in the United States, the Commissariat à l'Energie Atomique and the Centre National de la Recherche Scientifique/Institut National de Physique Nucléaire et de Physique des Particules in France, the Agenzia Spaziale Italiana and the Istituto Nazionale di Fisica Nucleare in Italy, the Ministry of Education, Culture, Sports, Science and Technology (MEXT), High Energy Accelerator Research Organization (KEK) and Japan Aerospace Exploration Agency (JAXA) in Japan, and the K. A. Wallenberg Foundation, the Swedish Research Council and the Swedish National Space Board in Sweden.

Additional support for science analysis during the operations phase is gratefully acknowledged from the Istituto Nazionale di Astrofisica in Italy and the Centre National d'Études Spatiales in France.

Facility: Fermi (LAT)

REFERENCES

Abdo, A. A., et al. 2009a, Phys. Rev. Lett., 103, 251101
Abdo, A. A., et al. 2009b, arXiv:0912.2040
Abdo, A. A., et al. 2009c, ApJ, submitted (arXiv:0912.4029)
Abdo, A. A., et al. 2009d, ApJS, 183, 46
Abdo, A. A., et al. 2009e, ApJ, 699, 817
Abdo, A. A., et al. 2009f, ApJ, 700, 597
Aharonian, F., et al. 2009, ApJ, 696, L150
Atwood, W. B., et al. 2009, ApJ, 697, 1071
Böttcher, M. 2007, Ap&SS, 309, 95
Böttcher, M., & Dermer, C. D. 2002, ApJ, 564, 86
D'Agostini, G. 2004, arXiv:physics/0403086
Dermer, C. D., & Schlickeiser, R. 1993, ApJ, 416, 458
Drury, L. O. 1991, MNRAS, 251, 340
Fichtel, C. E., et al. 1994, ApJS, 94, 551
Fields, B. D., Pavlidou, V., & Prodanović, T. 2008, Proc. 30th ICRC (Mexico City), 2, 153
Finke, J. D., Dermer, C. D., & Böttcher, M. 2008, ApJ, 686, 181
Ghisellini, G. 1989, MNRAS, 236, 341
Ghisellini, G., Celotti, A., Fossati, G., Maraschi, L., & Comastri, A. 1998, MNRAS, 301, 451
Ghisellini, G., Maraschi, L., & Tavecchio, F. 2009, MNRAS, 396, L105
Ghisellini, G., & Tavecchio, F. 2009, MNRAS, 397, 985
Hartman, R. C., et al. 1992, ApJ, 385, L1
Hartman, R. C., et al. 1999, ApJS, 123, 79
Kirk, J. G., & Mastichiadis, A. 1999, Astropart. Phys., 11, 45
Marcha, M. J. M., Browne, I. W. A., Impey, C. D., & Smith, P. S. 1996, MNRAS, 281, 425
Mattox, J. R., et al. 1996, ApJ, 461, 396
Sikora, M., Begelman, M. C., & Rees, M. J. 1994, ApJ, 421, 153
Sreekumar, P., et al. 1998, ApJ, 494, 523
Stocke, J. T., Morris, S. L., Gioia, I. M., Maccacaro, T., Schild, R., Wolter, A., Fleming, T. A., & Henry, J. P. 1991, ApJS, 76, 813
Strong, A. W., Moskalenko, I. V., & Reimer, O. 2004a, ApJ, 613, 962
Strong, A. W., Moskalenko, I. V., Reimer, O., Digel, S., & Diehl, R. 2004b, A&A, 422, L47
Urry, C. M., & Padovani, P. 1995, PASP, 107, 803
Vaughan, S., Edelson, R., Warwick, R. S., & Uttley, P. 2003, MNRAS, 345, 1271
Vercellone, S., et al. 2009, ApJ, 690, 1018
Vermeulen, R. C., Ogle, P. M., Tran, H. D., Browne, I. W. A., Cohen, M. H., Readhead, A. C. S., Taylor, G. B., & Goodrich, R. W. 1995, ApJ, 452, L5
Webb, G. M., Drury, L. O., & Biermann, P. 1984, A&A, 137, 185